ARCHIVES OF ELECTRICAL ENGINEERING VOL. 62(3), pp. 375-386 (2013)

DOI 10.2478/aee-2013-0030

An extended dynamic thermal model of a permanent magnet excited synchronous motor*

CHRISTELLE PIANTSOP MBO'O, KAY HAMEYER

Institute of Electrical Machines, RWTH Aachen University
Schinkelstr. 4, 52062 Aachen, Germany
e-mail: christelle.piantsop@iem.rwth-aachen.de

(Received: 26.06.2012, revised: 20.11.2012)

Abstract: The purpose of this paper is to develop a dynamic thermal model of a permanent magnet excited synchronous motor (PMSM). The model estimates the temperature at specific points of the machine during operation. The model is implemented using thermal network theory, whose parameters are determined by means of analytical approaches. Usually thermal models are initialized and referenced to room temperature. However, this can lead to incorrect results, if the simulations are performed when the electrical machine operates under "warm" conditions. An approach is developed and discussed in this paper, which captures the model in critical states of the machine. The model gives feedback by online measured quantities to estimate the initial temperature. The paper provides an extended dynamic thermal model, which leads to a more accurate and more efficient thermal estimation.

Key words: thermal modeling, thermal network, finite element method, iron losses, permanent magnet excited synchronous machine (PMSM)

1. Thermal network model

Thermal monitoring of electrical machines is required to highly utilize the electrical machine. A suitable thermal model allows a complete utilization of the thermal capacity of the machine and therefore an increase of power density. The temperature of the permanent magnet excited synchronous motors (PMSM) with buried rotor permanent magnets (Fig. 1) and equipped with a concentric winding in star-connection is modeled using a thermal network (Fig. 2) [1].

The network consists of heat sources (P), thermal resistances (R_{thi}) and capacitances (C_{thi}). Each element of the electrical machine, which is a heat source, is represented as a temperature node. The temperature nodes are: the housing (θ_1), the stator (θ_2), the slot windings (θ_3), the

* This is extended version of a paper which was presented at the 22th *Symposium on Electromagnetic Phenomena in Nonlinear Circuits*, Pula, Croatia, 26.06-29.06 2012.

end windings (θ_4), the permanent-magnets (θ_5) and the bearings (θ_6). The rotor is modeled by a parameter (magnet), which corresponds to the average rotor surface temperature. The thermal resistance between the ambient temperature and the housing R_{th1}, the housing and the stator R_{th2}, the stator and the slot windings R_{th3}, the slot windings and the end windings R_{th4}, the stator and the magnet $R_{th8,}$ the magnet and the bearings R_{th9}, the bearing and the housing R_{th10} depends on the thermal conductivity of the materials λ and the thickness of the layer t between the two solids.

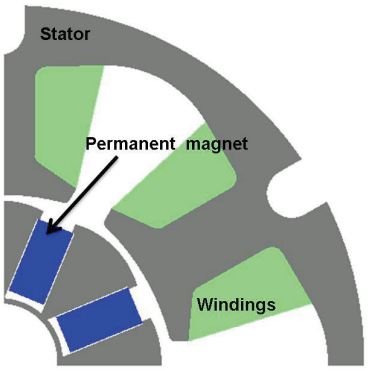

Fig. 1. Section of the PMSM

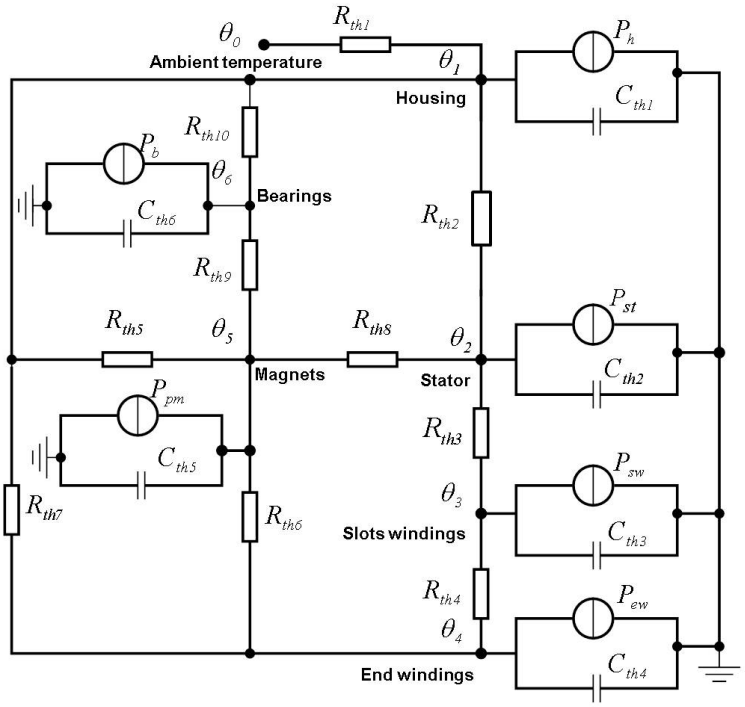

Fig. 2. Thermal network model

The analytical approach, presented in [1] is used to determine the value of these thermal resistances.

$$R_{th} = \frac{t}{\lambda \cdot A}. \tag{1}$$

There is a heat transfer by convection between the internal air and the housing, the end windings and the magnets. The thermal resistance of the internal air is enclosed to the thermal resistance $R_{th5,}$ $R_{th6,}$ R_{th7}. These resistances are determined by using the formula given in (2), whereas α is the convective heat transfer coefficient and A is the area of the radiated surface.

$$R_{th} = \frac{1}{\alpha \cdot A}. \tag{2}$$

The heat transfer coefficient of the air gap is derived from the Nusselt number Nu and the thermal conductivity of the airgap λ_{air}.

$$\alpha = \frac{Nu \cdot \lambda_{air}}{2 \cdot \delta}. \tag{3}$$

The heat transfer coefficient by convection for the end windings, the rotor and the housing are determined empirically. The resulted analytical expressions are proposed by [1], [2] and [3].

In addition to the thermal resistance, Figure 1 showed the thermal capacitances, which are required to simulate the transient state temperature distribution in the motor. Its value depends on the mass m_i and the specific heat capacity c_{pi} of the correspondant parts of the machine. It is calculated by (4), where i represents a node:

$$C_{thi} = m_i \cdot c_{pi}. \tag{4}$$

2. Dynamic thermal model

In order to estimate the temperature of each part of the machine, the machine losses have to be determined. Here, the losses consist of the ohmic losses ($P_{sw,}$ P_{ew}), the iron losses ($P_{st,}$ P_{pm}) and the bearing losses (P_b). The ohmic losses due to the stator currents in the slots P_{sw} and in the end windings P_{ew} are determined according to the variation of temperature of the slot θ_3 and the end windings θ_4.

$$P_{sw,\,ew} = 3 \cdot R(\theta_{3,4}) \cdot I^2. \tag{5}$$

The iron losses of the stator P_{st} consist of the hysteresis losses P_h, the eddy-current losses P_{ec} and the excess losses P_{ex} [4]. These are computed using a transient 2D-FE approach and a post processing formula defined in [5] and [6]. According to which the eddy-current losses and the excess losses are computed from the contribution of each harmonic of the flux density over one electrical period in time. The hysteresis losses are computed as a function of the peak

value of the magnetic flux density over the same period. Each types of the iron losses of the motor are calculated using the FE-approach for some value of the current by the rated speed. Figure 2 shows the distribution of the losses by field weakening.

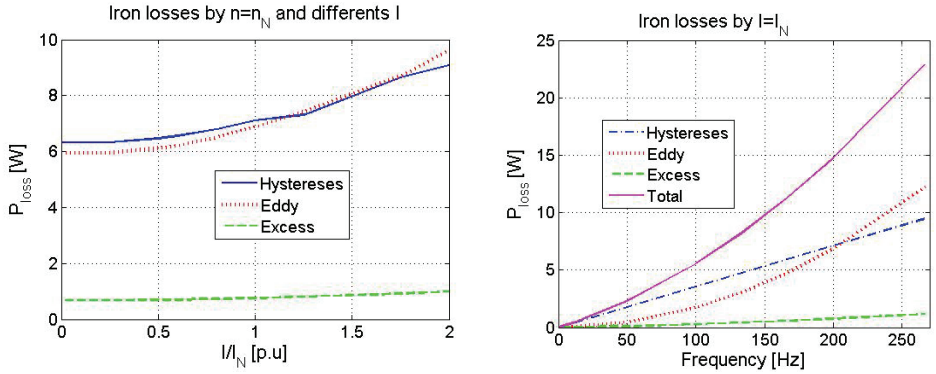

Fig. 3. Iron losses of the stator by field weakening (left) and by different frequency (right)

The values of the losses by field weakening are integrated in the losses model as a look-up table (LUT). To estimate the losses at each operating point, the value is taken from the LUT by the corresponding current and rescale to the corresponding speed using the formulation (6).

$$P_{st} = P_{h,n_N} \cdot \frac{f}{f_N} + P_{ex,n_N} \cdot \left(\frac{f}{f_N}\right)^{1.5} + P_{ec,n_N} \cdot \left(\frac{f}{f_N}\right)^{2}. \tag{6}$$

The iron losses of the magnets (NdFe) P_{pm} consist mainly of the eddy-current losses. The eddy-current density is calculated by means of a transient 3D-FE approach. It is integrated over the magnets volume and multiplied with their specific conductivity to estimate the losses (7).

$$P_{pm} = \frac{1}{\sigma_{pm}} \cdot \int J_{ec}^2 \cdot dV_{pm}. \tag{7}$$

The iron loss of the stator and the eddy current loss of the permanent magnet related to the current and the speed of the machine are shown on Figure 4.

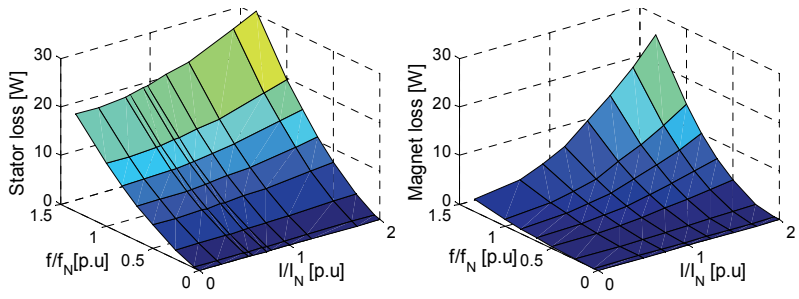

Fig. 4. Total iron loss of the stator and eddy current loss of the permanent magnet

The bearing loss P_b is calculated from the linear approximation of the total bearing loss at the maximum speed ($n_{\max}$). This was given from the machine supplier.

$$P_b(n) = P_{b,n_{\max}} \cdot \frac{n}{n_{\max}}. \tag{8}$$

After the computation of the losses, the thermal resistances and capacitances, the temperature of each node is computed by solving the differential equation system given as:

$$C_{th} \cdot \dot{\theta}(t) = G \cdot \theta(t) + P_{loss}(t). \tag{9}$$

Whereas C_{th} is the diagonal capacitance matrices, G is the symmetric matrix of thermal conductance and P_{loss} is a vector that contains the losses values at each machines parts.

The differential equations system is presented in the state space form:

$$\dot{\theta}(t) = A \cdot \theta(t) + B \cdot P_{loss}(t) \cdot \theta(t), \tag{10}$$

$$y = C \cdot \theta(t) \tag{11}$$

with $A = -C_{th}^{-1} \cdot G; \quad B = C_{th}^{-1}$. C represents the relationship between the estimated values and the output of the system. The system was implemented in Matlab/Simulink and the model is presented in Figure 5.

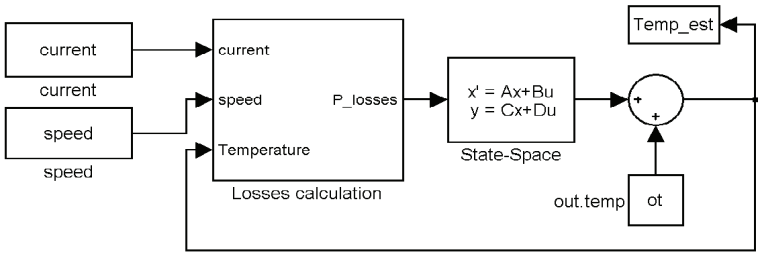

Fig. 5. The dynamic thermal model

The input parameters of the model are the current, the speed and the ambient air temperature (*ot*). The model consists of a subsystem for the losses estimation, in which the ohmic losses are calculated from a closed-loop using the winding temperature, the iron losses and the magnet losses are integrated as described above.

3. Extended model

The model is now extended with an initialization, that provides initial state when the system is restarts. The initialization receives as input in addition to the ambient temperature, the housing temperature (Fig. 6).

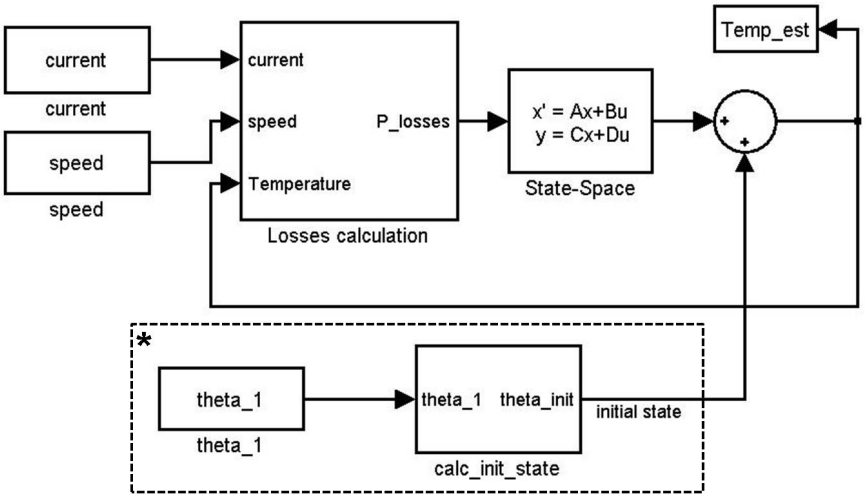

Fig. 6. Extended dynamic thermal model. (*) This part is not inside the model. It is used once in the beginning for the initialization

When the system is stopped, the machine begins to cool down. The differential equations system is reduced to:

$$C_{th} \cdot \Delta\theta = G \cdot \theta. \tag{12}$$

Whereas $\Delta\theta$ is a constant value, that was calculated from the measured values. The expression in (12) gives a linear equation system of 6 equations.

This was reduced in 3 equations, by expressing the slots windings and the bearings temperature as a function of the housing, the stator, the end windings and the magnet temperature.

The initial temperature of the node: θ_2, θ_4, θ_5 are given by solving the expression:

$$A_s \cdot \begin{bmatrix} \theta_2 \\ \theta_4 \\ \theta_5 \end{bmatrix} = B_s, \tag{13}$$

$$A_s = \begin{bmatrix} G(1,2) & G(1,4) & G(1,5) - \dfrac{G(1,6)\cdot G(6,5)}{G(6,6)} \\ G(2,2) - \dfrac{G(2,3)\cdot G(3,2)}{G(3,3)} & \dfrac{G(2,3)\cdot G(3,4)}{G(3,3)} & G(2,5) \\ -\dfrac{G(4,3)\cdot G(3,2)}{G(3,3)} & G(4,4) + \dfrac{G(3,4)\cdot G(4,3)}{G(3,3)} & G(4,5) \\ G(5,2) & G(5,4) & G(5,5) + \dfrac{G(5,6)\cdot G(6,5)}{G(6,6)} \end{bmatrix} \tag{14}$$

$$B_s = \begin{bmatrix} \left(G(1,1) - \dfrac{G(1,6)\cdot G(6,1)}{G(6,6)}\right)\cdot\theta_1 + C(1)\cdot\Delta\vartheta_1 - \dfrac{G(1,6)\cdot C(6)\cdot\Delta\theta_6}{G(6,6)} \\ G(2,1)\cdot\theta_1 + C(2)\cdot\Delta\vartheta_2 \\ G(4,1)\cdot\theta_1 - \dfrac{G(4,3)\cdot C(3)\cdot\Delta\theta_3}{G(3,3)} + C(4)\cdot\Delta\theta_4 \\ \left(G(5,1) - \dfrac{(G(5,6)\cdot G(6,1)}{G(6,6)}\right)\cdot\theta_1 + C(5)\cdot\theta_5 - \dfrac{G(5,6)\cdot C(6)\cdot\Delta\theta_6}{G(6,6)} \end{bmatrix} \tag{15}$$

The slots winding and the bearings temperature is given as:

$$\theta_3 = -\frac{G(3,4)}{G(3,3)}\cdot\theta_4 - \frac{G(3,2)}{G(3,3)}\cdot\theta_2, \tag{16}$$

$$\theta_6 = -\frac{G(6,1)}{G(6,6)}\cdot\theta_1 - \frac{G(6,5)}{G(6,6)}\cdot\theta_5. \tag{17}$$

4. Model evaluation

The test motor is a self-cooling permanent magnet synchronous motor with star-connected concentric winding. The star connector is not available. The motor properties are listed on the Table 1.

Table 1. Data sheet of the testmotor

Rated value	Numerical value
Torque M_N	1.35 Nm
Speed n_N	3000 rpm
Power P_N	425 W
Voltage U_N	230 V
Current I_N	2.3 A

To evaluate the model, five temperature sensors are placed at the end windings (drive-side and shaft-end), in the slots windings (top and bottom) and at the housing of the tests motors.

The thermal resistances R_{th1} and R_{th3} have a great influence on the estimated temperature. These values may not exactly be determined using the analytical approach because of probable manufacturing tolerances and an unusual stator shape of the motor. For this purpose, the motor with a locked rotor is fed by the nominal direct current and heated up to thermal steady-state. The total losses and the temperature of the housing are used to determine R_{th1}. The thermal resistance R_{th3} has varied until the simulated end windings temperature matches the measured values. The model is simulated with the calculated values of R_{th1} and R_{th3}.

The simulated temperature rise in comparison to the measured one is plotted in Figure 6. The mean value of the end windings temperature and the slot windings temperature is com-

pared to the simulated data.

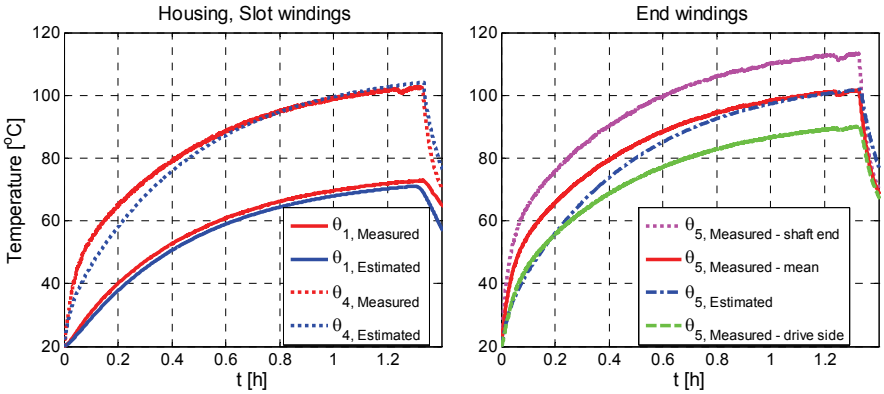

Fig. 7. Temperature rise by locked rotor operation

The Table 2 illustrate the temperature at the steady state. This model shows a maximum deviation at the steady state from 3% in comparison to the measured data.

Table 2. Comparison of the result at the steady state

Temperature nodes	**Measured** [°C]	**Simulated** [°C]
Housing θ_1	72.82	71.06
Slot winding θ_3	102.93	104.16
End windings θ_4	101.77	101.92

The dynamic thermal model is now evaluated by intermittent operation. The motor is driven in an intermittent operation by 2000 rpm and 1Nm. The motor was warm at the beginning and the ambient temperature was 22°C. The motor was operated three times for max. 500 s and twice at stand still for max. 1000 s. The Figure 8 shows the temperature rise of the motor. There is a large deviation (5°C-7°C) between the first estimated value and the measured ones.

Figure 9 represents the current and the mechanical power of the system during the intermittent operation.

During the continuous operation, the motor was in cold condition. The simulated value at the beginning of the measurement was very close to the measured one. However after restarting the system, when the motor is warm, there is a large deviation between the estimated value and the measured one.

According to the presented results above, the model delivers good results as long as the motor is cold at the beginning of the estimation.

To improve the estimation, the model was extended with an initialization. The initial temperature was calculated for the intermittent operation and the extended model is used to estimate the temperature. The initial temperature was compared with the measured one in Table 3.

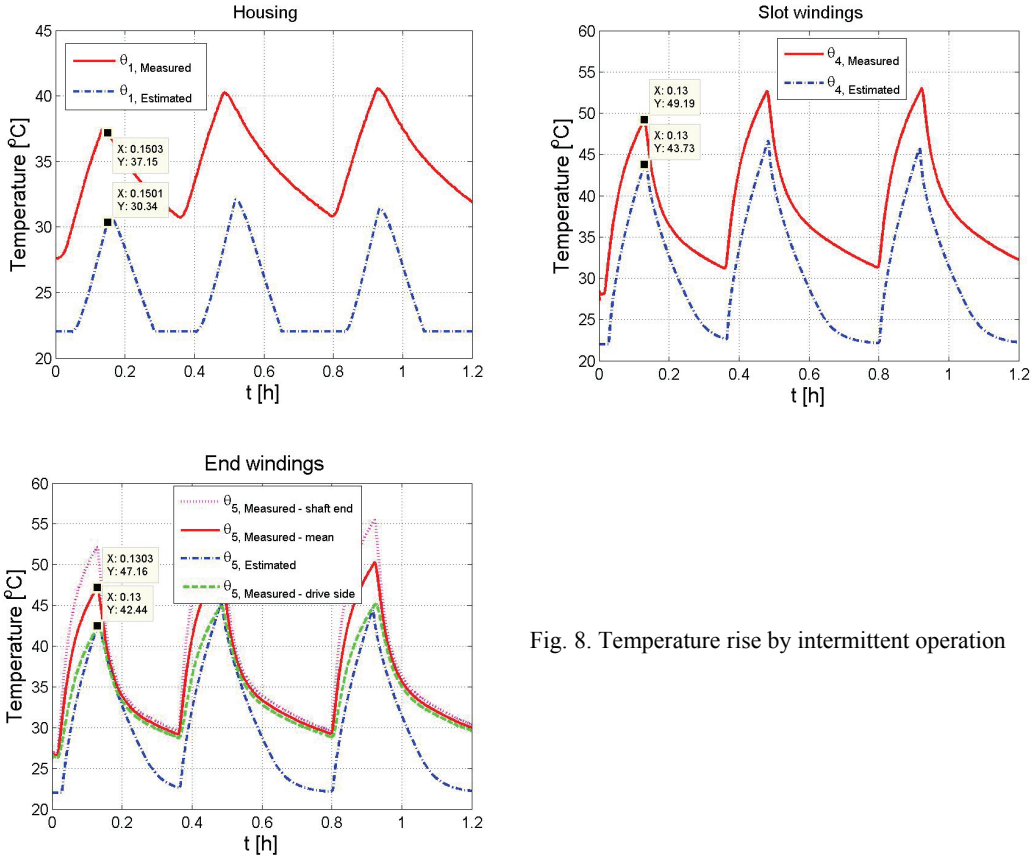

Fig. 8. Temperature rise by intermittent operation

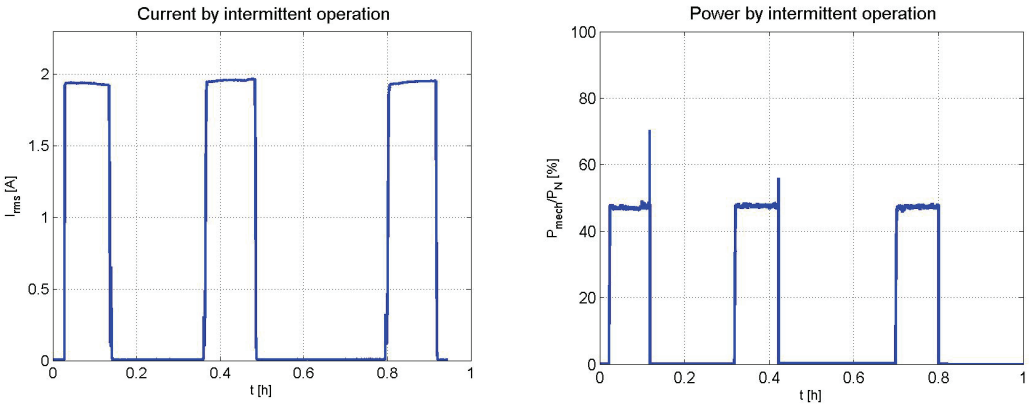

Fig. 9. Mean values of the current (left) and mechanical power by intermittent operation (right)

The Figure 10 shows the temperature rise during the first operation with the initial state until the second and the third stage is reached. There is a small deviation at the beginning between the measured values and the simulated ones.

Table 3. Comparison of the result at the beginning

Temperature nodes	Measured [°C]	Simulated [°C]
Housing θ_1	27.64	27.64
Slot winding θ_3	28.60	27.74
End windings θ_4	28.20	27.84

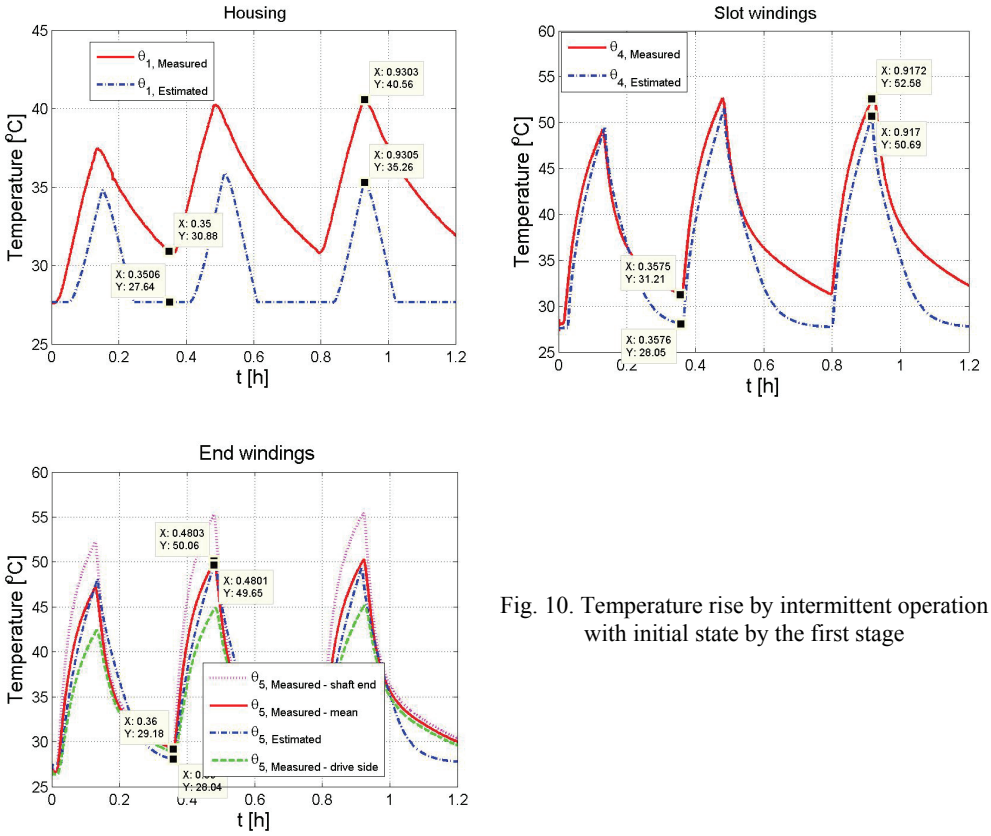

Fig. 10. Temperature rise by intermittent operation with initial state by the first stage

The Table 4 presents the comparison of the results after 500 s.

Table 4. Comparison of the result after 500 s

Temperature nodes	Measured [°C]	Simulated [°C]
Housing θ_1	37.38	35.42
Slot winding θ_4	49.75	49.2
End windings θ_5	47.11	48.44

During the second and the third working stage, the deviation is increased (max. 5°C). Because of this, the model was reinitialized after the first stage. The simulation results of the second stage after the re-initialization is demonstrated in Figure 11.

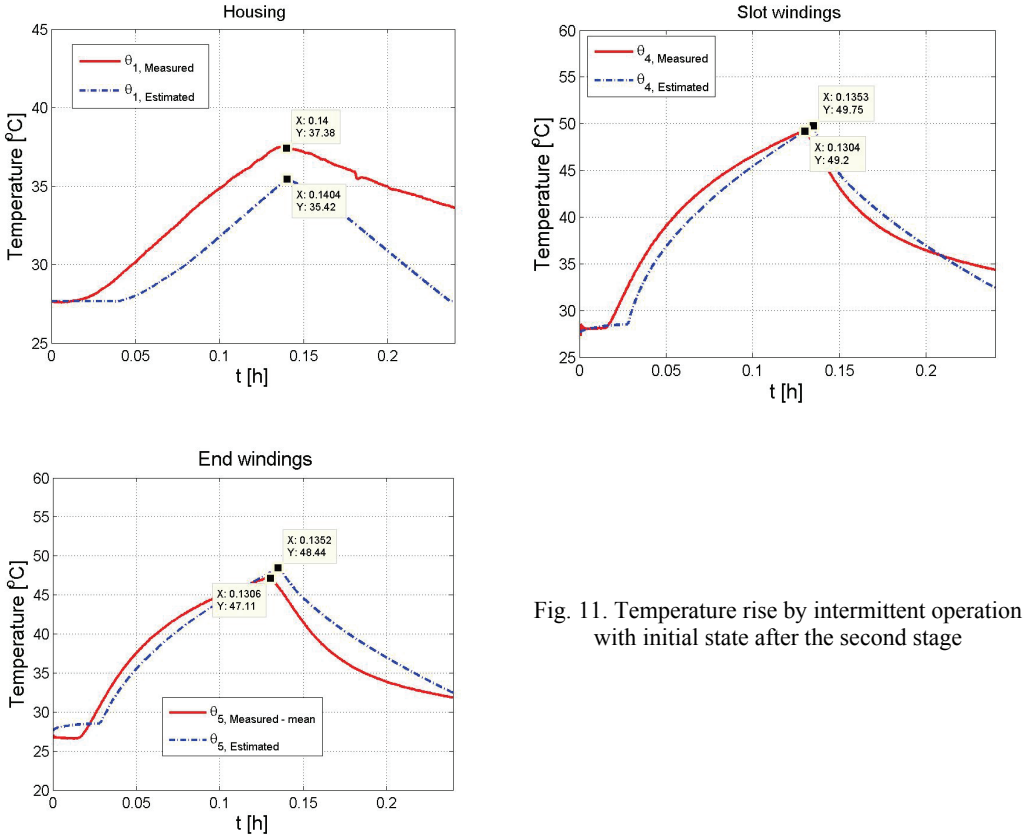

Fig. 11. Temperature rise by intermittent operation with initial state after the second stage

The simulations results present a maximum deviation of 3°C.

5. Conclusions

This contribution presents a dynamic thermal network model of a PMSM and its limitation in the case of an unexpected operation. The main part of the paper discusses the computation of the thermal resistances, capacitances and heat losses. The dynamic thermal model was extended by an initialization to estimate the initial state of the machine at every restarting of the system. The extended model provides a more accurate and more efficient temperature estimation.

References

[1] Lindstroem J., *Thermal Model of a Permanent Magnet Motor for a Hybrid Electric Vehicle*. Department of Electric Power Engineering, Chalmers University of Technology Göteborg, Sweden (1999).

[2] Kylander G., *Thermal modelling of small cage induction motors.* PhD. Dissertation, School of Electrical and Computer Engineering, Chalmers University of Technology Göteborg, Sweden, Tech. Report. 265 (1995).

[3] Demetriades G.D., de la Parra H.Z., Andersson E., Olsson H., *A real-time thermal model of a permanent magnet synchronous Motor*. IEEE Transactions on Power Electronics 25(2): 463-474 (2010).
[4] Bertotti G., Boglietti A., Chiampi M. et al. *An improved estimation of iron losses in rotating electrical machines.* IEEE Trans. Magn. 27(6): 5007-5009 (1991).
[5] Gracia M.H., Lange E., Hameyer K., *Numerical calculation of iron losses in electrical machines with a modified post-processing formula*. Proceedings of the 16th International Symposium on Electromagnetic Fields COMPUMAG, Aachen, Germany (2007).
[6] Jacobs S., Hectors D., Henrotte F. et al. *Magnetic material optimization for hybrid vehicle PMSM drives.* EVS24-International Battery, Hybrid and Fuel Cell Electric Vehicle Symposium, Stavanger, Norway (2009).